

On the magnetosensitivity of lipid peroxidation: Two- versus three-radical dynamics: Supporting Information

Chris Sampson¹, Robert H. Keens¹, and Daniel R. Kattnig¹

¹Living Systems Institute and Department of Physics, University of Exeter, Stocker Road, Exeter, Devon, EX4 4QD, United Kingdom

Contents

1	Comments on the model	1
1.1	Assessment of lateral diffusive motion	1
1.2	Assessment of spin relaxation	2
2	Calculation of the g-tensor	2
3	Calculating the Hyperfine Interactions	2
4	Reactivity of the Third Radical (C)	9
5	Three-radicals only coupled by hyperfine interactions	10
6	Anisotropies of the MFE	11
7	Dependence on the orientation of the magnetic field	12
8	Microreactors	13

1 Comments on the model

1.1 Assessment of lateral diffusive motion

To our knowledge, no data exist regarding the diffusion of lipid radical peroxides in membranes. However, it has been shown that the diffusion coefficients for stable radical molecules are similar to those of the non-radical molecules, whereas unstable radical molecules have been shown to diffuse slower than their non-radical counterparts [1, 2]. In a review by Macháň *et al.* [3], diffusion coefficients for lipids in giant unilamellar vesicles are reported to range from $1.4 \mu\text{m}^2\text{s}^{-1}$ to $7 \mu\text{m}^2\text{s}^{-1}$. However, they are expected to be significantly smaller in actual biological environments. As lipid peroxides are relatively stable radicals [4] that are a similar in size to lipids, we approximate that the radical species would diffuse at a rate comparable to that of its non-radical precursor. Based on these facts, we estimate that lipid peroxides will undergo a diffusive displacement of significantly less than the free Brownian diffusion length $L_D = \sqrt{4Dt}$ calculated with the above diffusion coefficients. A characteristic time t can be estimated based on a typical spin relaxation time of an organic radical, because all MFE have to manifest within the lifetime of the pertinent spin coherences (*vide infra*). Assuming a coherent lifetime of 100 ns, we thus estimate a lateral displacement of less than 1.7 to 0.7 nm. Therefore, in good approximation, we shall neglect diffusion during the timespans that give rise to the formation of the MFE in a biological membrane.

1.2 Assessment of spin relaxation

MFEs are expected if the spin and reaction dynamics occur on time-scales that are faster or comparable to spin relaxation times. Thermalized spin systems cannot convey magnetosensitivity to weak magnetic fields, because the Zeeman interaction energy is small compared to the thermal energy, $k_B T$, and, thus, equilibrium properties are negligibly affected. Alkyl peroxy radicals in free solution are subject to fast spin relaxation as a consequence of large g -anisotropies, which facilitates efficient spin rotational relaxation [5]. Consequently, EPR spectra of alkyl peroxy radicals in liquid solution at room temperature are typically broad [6,7]. Yet, an order of magnitude estimate suggests that spin rotation will likely not impact the MFEs of lipid peroxy reactions in membranes for short-lived, i.e. reactive, encounters, because the deviations of the g -tensor principal values from the g -factor of the free electron are sufficiently small and the motional correlation time is sufficiently long. This argument is based on the rotational diffusion rates from [8] ($D_{\parallel} = 1 \times 10^7 \text{ s}^{-1}$ and $D_{\perp} = 1 \times 10^8 \text{ s}^{-1}$) to estimate a typical motional correlation time of the lipid (using $\tau_c = 1/(4D_{\perp} + 2D_{\parallel}) \sim 2 \text{ ns}$) and

$$T_1^{-1} = T_2^{-1} = \frac{1}{9\tau_c} \sum_{a \in \{x,y,z\}} (g_{aa} - g_e)^2 \quad (1)$$

to evaluate the order of magnitude of the spin rotational relaxation rates. Here, the g_{aa} s are the principal values of the g -tensor. With g -parameters calculated using DFT, our estimate suggests spin relaxation times exceeding $10 \mu\text{s}$. While this estimate is based on a simplified view of molecular dynamics that neglects internal degrees of freedom, it shows that even motions that are faster by two orders of magnitude will not suppress the MFEs discussed here (for an assumed maximal encounter time of 100 ns). Unfortunately, we are not aware of a detailed motional model that would allow us to estimate internal motion at the current stage. In order to put this in context, note that, for the same τ_c , the superoxide radical anion is expected to relax faster by a factor of 33. It is important to realize that our assessment applies to the scenario that all radicals are lipid bound. The cage reaction suggested in [9] involved a free hydroxyl radical, the fast relaxation of which almost certainly abolishes MFEs due to the RPM for moderate field intensities (estimated relaxation time: 1 ns [10], which is consistent with the EPR line width in [11]).

2 Calculation of the g -tensor

The g -tensor was calculated for the most stable conformer of the radical isomer 9ez using the Gaussian16 software. The unrestricted B3LYP exchange-correlation functional was used with a Def2TZVP basis set and a tight convergence criterion for the SCF iterations. This approach yielded the following shifts relative to the free electron g -factor:

Table S1: g -tensor shifts relative to the free electron (ppm)

XX	YY	ZZ
-304.2	5961.6	27887.8

3 Calculating the Hyperfine Interactions

The hyperfine coupling constants of two isomers of linoleic acid peroxy radical, 13ze and 9ez, as described in the main text, were calculated by DFT using NWChem 6.8.1. The dihedral angle that the peroxy group makes with the backbone chain was scanned from -180 to 180° with

38 points. At each dihedral angle a geometry optimisation was performed while holding the selected dihedral angle constant. Each simulation used the def2-tzvp basis set with the exchange-correlation functional B3LYP, an SCF threshold of 1×10^{-8} and the xfine grid. Using the resultant optimised structures, the hyperfine values were calculated using the same exchange-correlation functional with the EPR-III basis. The largest hyperfine coupling constant was found for the hydrogen vicinal to the peroxide group.

Fig. S1A shows the dependence of the isotropic hyperfine constants on the peroxy dihedral angle for several hydrogen atoms of interest in the 9ez and 13ze isomers. There is evidently a large range of values a_{iso} can take depending on the orientation of the dihedral angle. To calculate the average interaction, a Boltzmann average was calculated. The potential energy surface for this rotation is shown in Fig. S1B. With these data, the Boltzmann-weighted average hyperfine coupling tensor $\langle \mathbf{A} \rangle$ can be calculated from

$$\langle \mathbf{A} \rangle = \sum_i z_i \mathbf{A}_i, \quad (2)$$

$$z_i = \frac{e^{-\Delta E_i/(k_B T)}}{\sum_j e^{-\Delta E_j/(k_B T)}}, \quad (3)$$

where \mathbf{A}_i is the hyperfine tensor of conformation i after alignment of the backbone (carbons 1 to 8) to the minimal energy configuration. E_i is the potential energy of the i^{th} orientation associated with the dihedral angle, k_B is the Boltzmann constant and T is the temperature. Here, we used a temperature of 310 K to be in line with temperatures within biological systems. By following this method, a_{iso} associated with 13ze was calculated to be 10.3 MHz. An equivalent process was followed for 9ez to produce an a_{iso} of 13.5 MHz.

Tables S2 and S3 show the largest anisotropic hyperfine coupling constants when the Boltzmann-weighted average is calculated. In both isomers the isotropic constants are all below 1 MHz with the exception of the hydrogen bonded to the same carbon as the peroxide group, where the hyperfine coupling constants increase substantially to over 10 MHz.

We do not consider the anisotropic hyperfine constants in the main section of the article. However, we show their magnitudes and signs in Fig. S2. When the rotation of the lipid about its backbone is considered, the anisotropy is strongly reduced. This is shown in Fig. S3. As the anisotropy fades with molecular motion, the isotropic model is an appropriate approximation to make for this system.

Figure S1: A: Isotropic hyperfine coupling constants as the peroxide group rotates around the dihedral angle made with the backbone of the lipid. Each atom label corresponds to a hydrogen within each lipid peroxide radical where the number represents the carbon number on the backbone. B: Potential energy surface as the peroxide group rotates around the dihedral angle made with the backbone of the lipid.

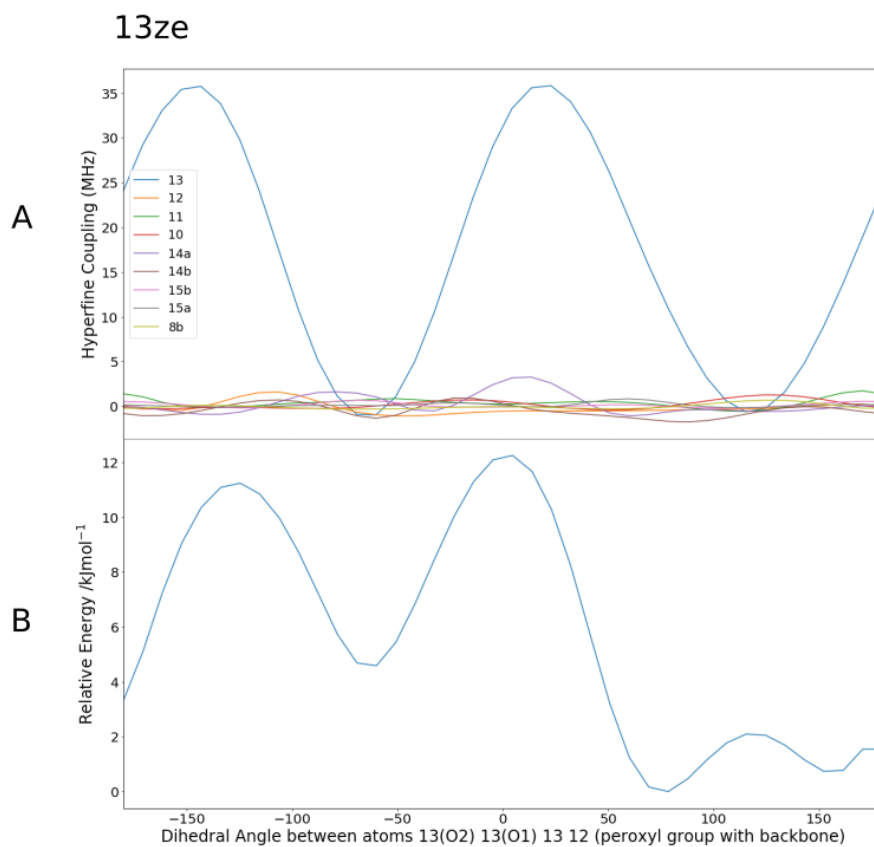
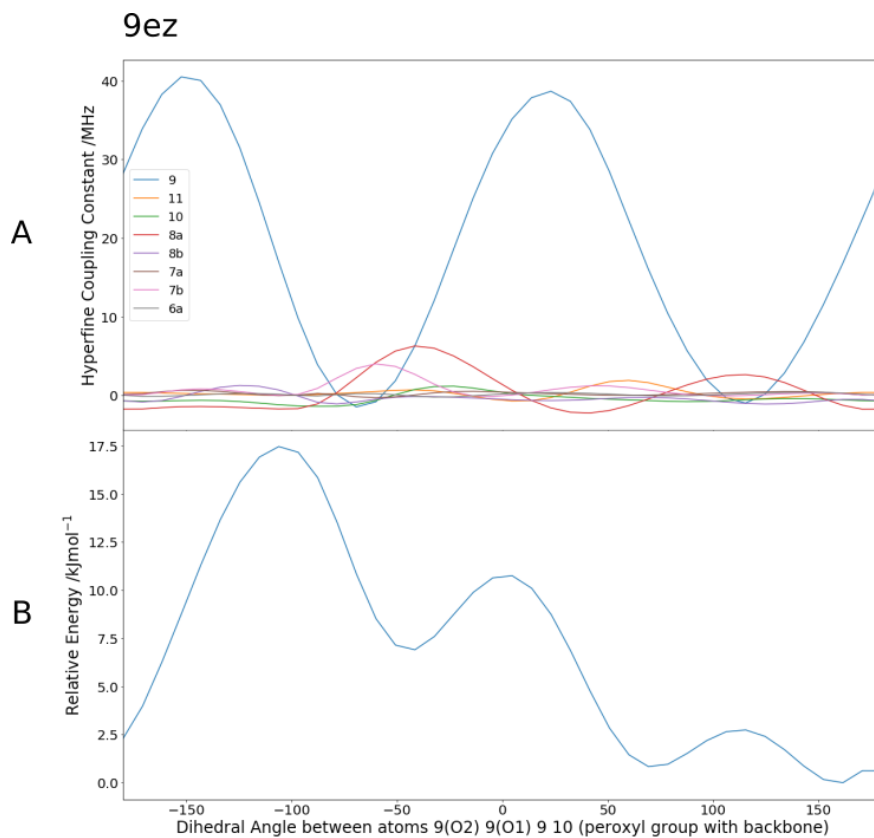


Table S2: 9ez hyperfine coupling constants. Each atom label corresponds to a hydrogen within each lipid peroxide radical where the number represents the carbon number on the backbone.

Atom Number	a_{iso} (MHz)	anisotropy (MHz)	asymmetry
6a	0.155	1.52	0.00805
5b	-0.008	2.11	0.0327
7a	0.225	3.93	0.0286
7b	0.371	8.03	0.0493
8b	-0.602	8.65	0.188
8a	0.103	4.39	0.105
10	-0.561	9.44	0.135
11	0.441	2.44	0.0878
12	0.008	1.67	0.0482
9	13.488	14.9	0.0465

Table S3: 13ze hyperfine coupling constants. Each atom label corresponds to a hydrogen within each lipid peroxide radical where the number represents the carbon number on the backbone.

Atom Number	a_{iso} (MHz)	anisotropy (MHz)	asymmetry
8a	-0.005	1.70	0.0234
15a	0.223	2.29	0.0537
15b	0.137	2.78	0.0747
16a	-0.024	1.61	0.0608
14b	-0.925	10.1	0.166
14a	-0.343	6.49	0.0951
10	0.353	1.21	0.0488
11	0.372	2.98	0.0567
12	-0.238	8.01	0.158
13	10.317	14.6	0.0385

Figure S2: Average hyperfine coupling tensors when the dihedral angle describing the orientation of the peroxy group fluctuates in the potential given by Fig. S1 for 13ze (left) and 9ez (right). Blue indicates positive and green negative hyperfine components in the respective direction.

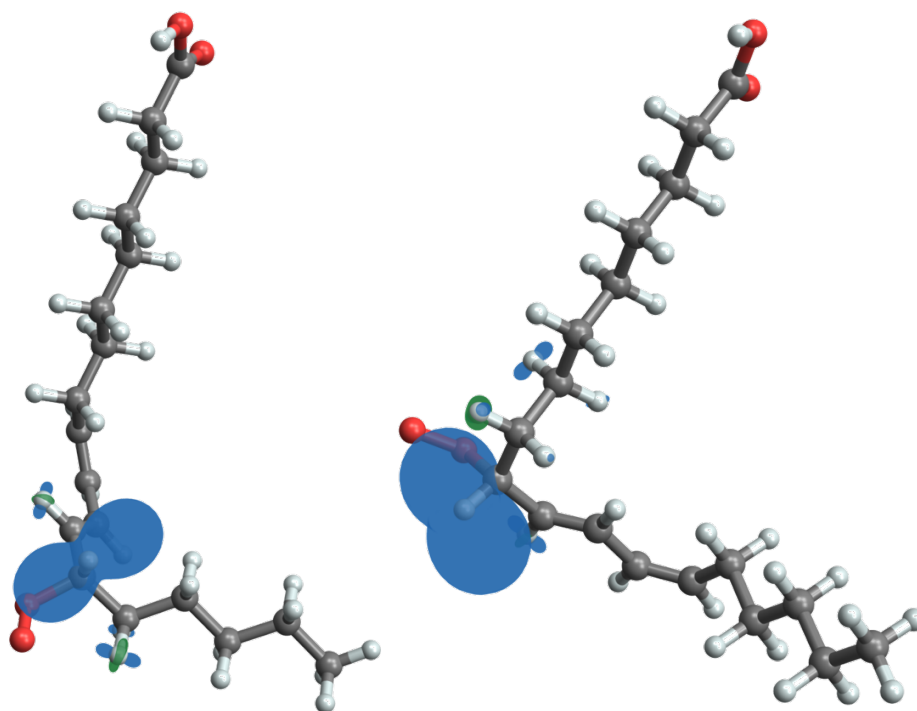


Figure S3: 13ze (left) and 9ez (right) shown with the average hyperfine interaction on the vicinal hydrogen when it is averaged by fast rotation about the carbon backbone (axis of rotation indicated by the black line) in addition to the fluctuations of the orientation of the peroxy group.

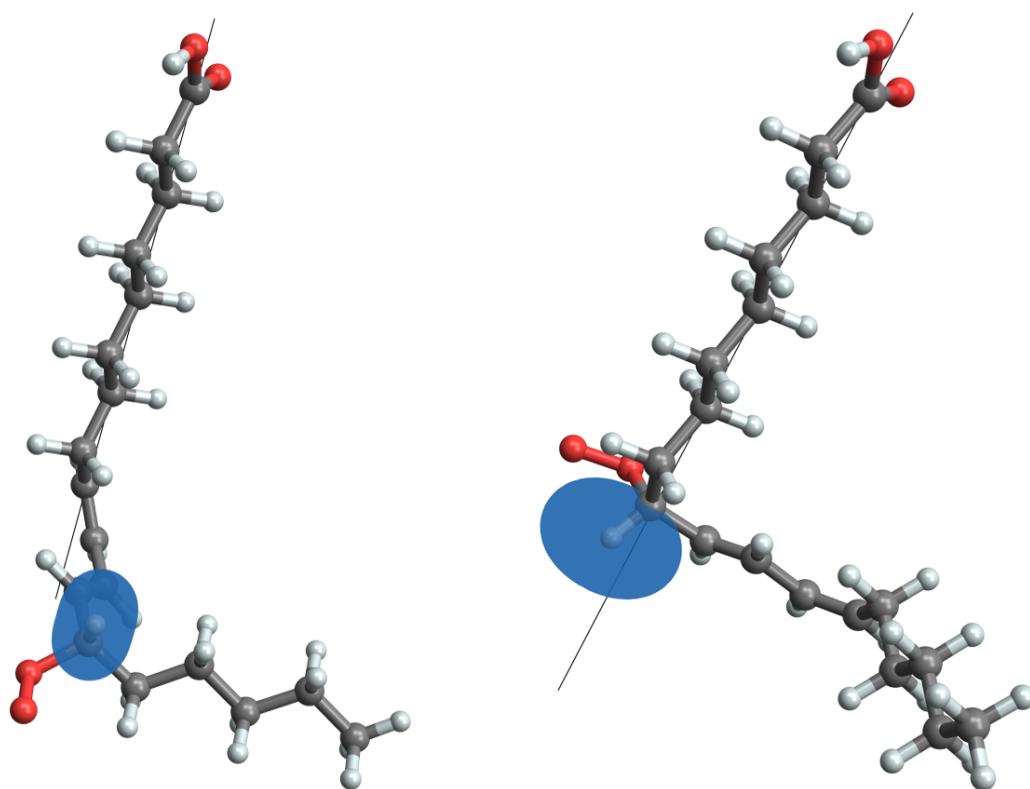
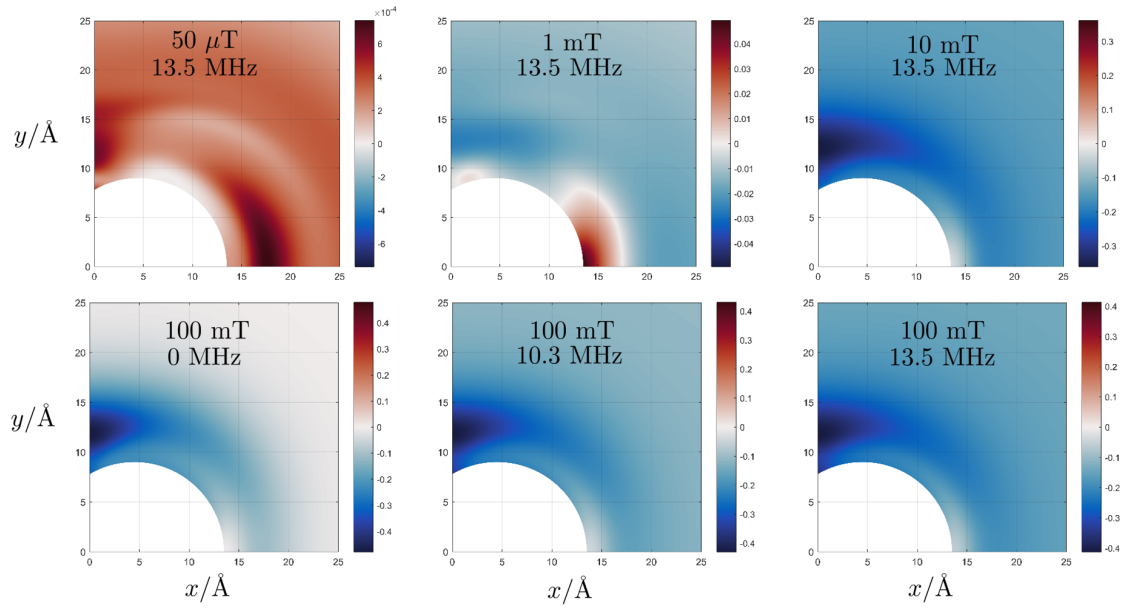


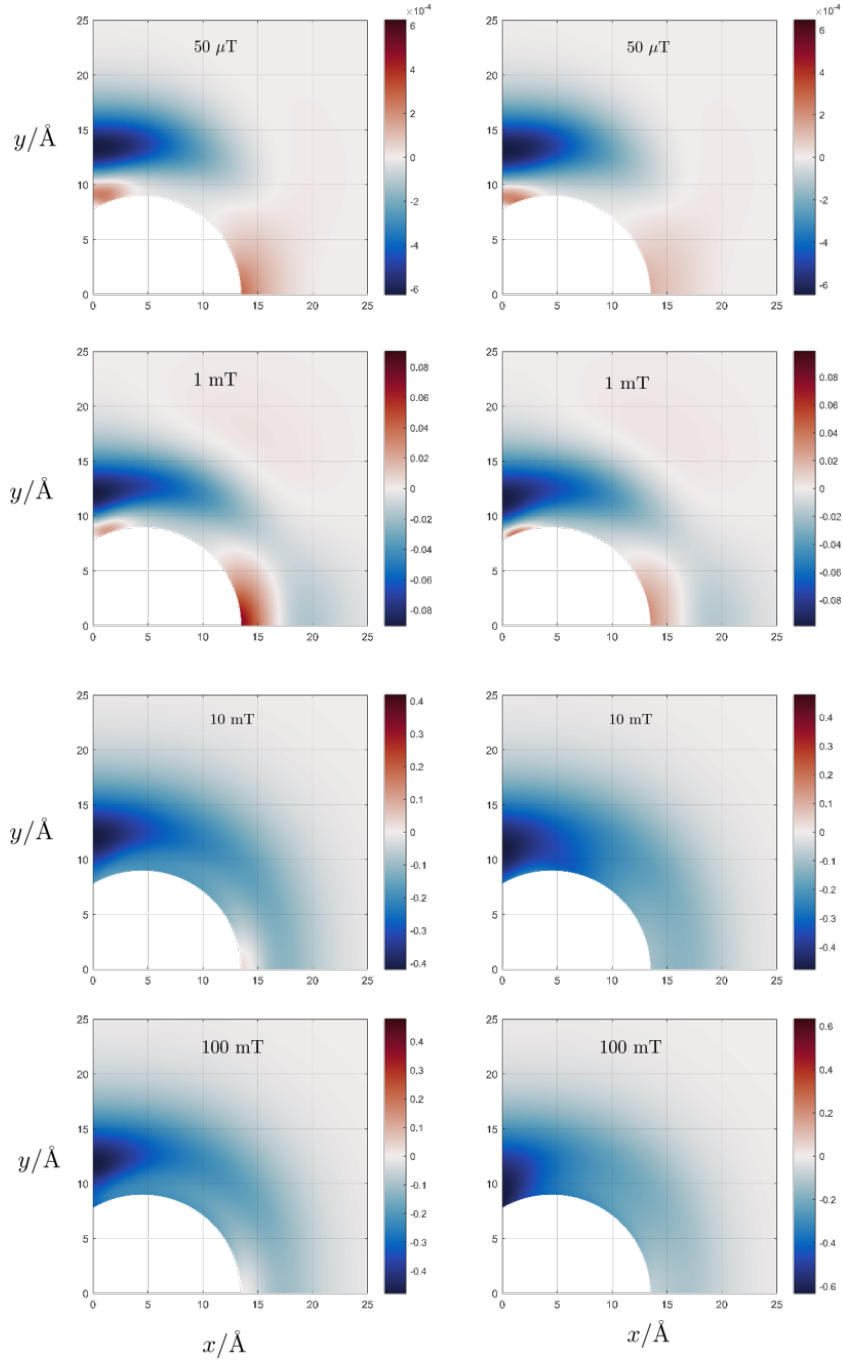
Figure S4: Magnetic field effects (χ_P) for three-radical systems when the magnetic field is perpendicular to the plane of the membrane. The strength of the magnetic field and the value of the hyperfine coupling constant used is shown in each graph. For all calculations $J = 0$, $k_{P,0} = 0.2 \text{ ns}^{-1}$ and $k_e = 0.01 \text{ ns}^{-1}$.



4 Reactivity of the Third Radical (C)

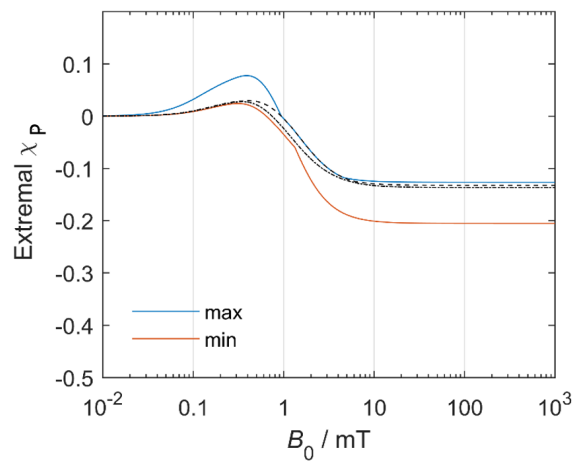
Although we have used a single value of $k_{P,0}$ for all pairs of radicals throughout the main text, we show here that minimal difference occurs by assuming that the third radical is unreactive. Fig. S5 shows the results, when a reactive C (left) or an unreactive C (right) is used. The results appear to be largely insensitive to the level of reactivity of the third radical, with only minor differences such as the magnitude of the MFE at contact when using $B_0 = 1$ mT. The location of the MFE, however, does not change in any significant way.

Figure S5: MFEs when the third radical (C) is reactive (left) and unreactive (right) for different magnetic field strengths. The magnetic field is perpendicular to the membrane plane. The parameters are as follows: $J = 0$, $k_{P,0} = 0.2 \text{ ns}^{-1}$, $k_e = 0.01 \text{ ns}^{-1}$ and $a_{iso} = 10.3 \text{ MHz}$.



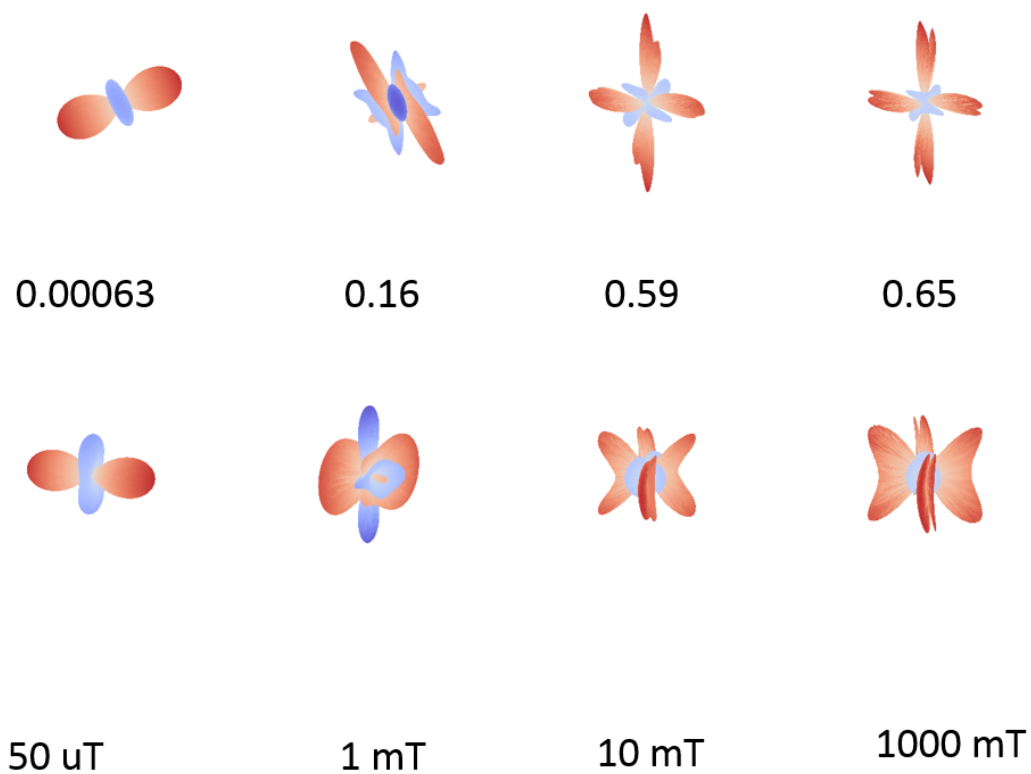
5 Three-radicals only coupled by hyperfine interactions

Figure S6: Magnetic field effects (χ_P) for a three-radical system when the HFI is included, but EED is excluded. Parameters: $a_{iso} = 10.3$ MHz, $J = 0$, $k_{P,0} = 0.2$ ns $^{-1}$ and $k_e = 0.01$ ns $^{-1}$.



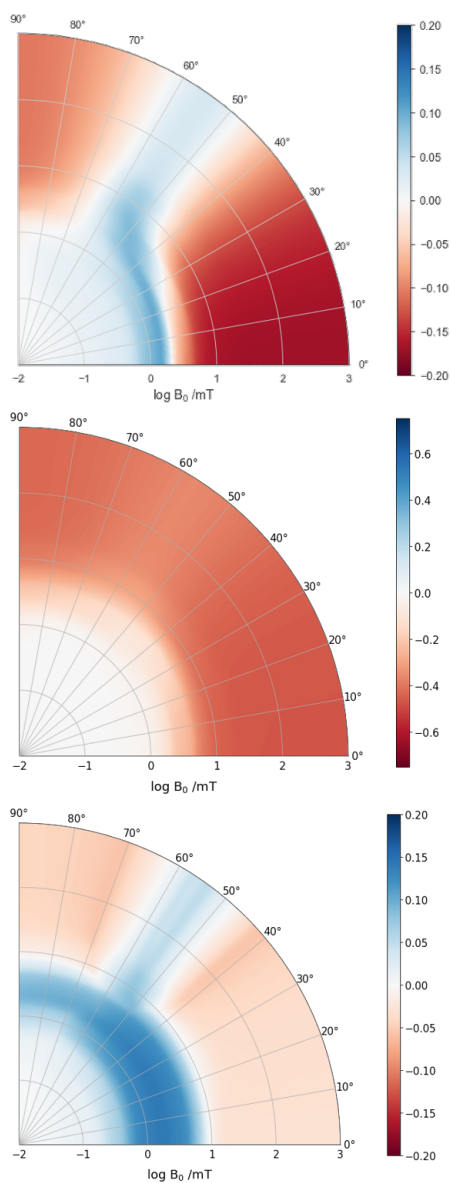
6 Anisotropies of the MFE

Figure S7: Plots of the anisotropies of the MFEs of a three-radical system for 50 μT (left), 1 mT (middle-left), 10 mT (middle-right), 1000 mT (right). The top and bottom show the same image from different angles and the numbers indicate the anisotropies (%). Parameters are as follows: $k_{P,0} = 0.2 \text{ ns}^{-1}$, $k_e = 0.01 \text{ ns}^{-1}$, $J = 0$, $a_{iso} = 0$, $|\mathbf{r}_{1,3}| = 13.7 \text{ \AA}$, $|\mathbf{r}_{2,3}| = 15.5 \text{ \AA}$.



7 Dependence on the orientation of the magnetic field

Figure S8: Dependence of the MFE on the orientation of the magnetic field. The field is rotated from parallel with z -axis to parallel with x -axis. Top: two-radical, middle and bottom: three-radical system. Dipolar and hyperfine interactions are included, the latter with a coupling constant of 10.3 MHz. Middle shows the minimum possible MFE and the bottom shows the maximum possible MFE for variable positions of the third radical.



8 Microreactors

Figure S9: The magnetic field at which the MFE reaches half saturation plotted against the surface concentration of the lipids. The blue and red lines represent the cases with $a = 0$ and $a = 10.3$ MHz, respectively, both with the magnetic field oriented perpendicular to the membrane plan. The yellow line shows the rotational average when $a = 0$.

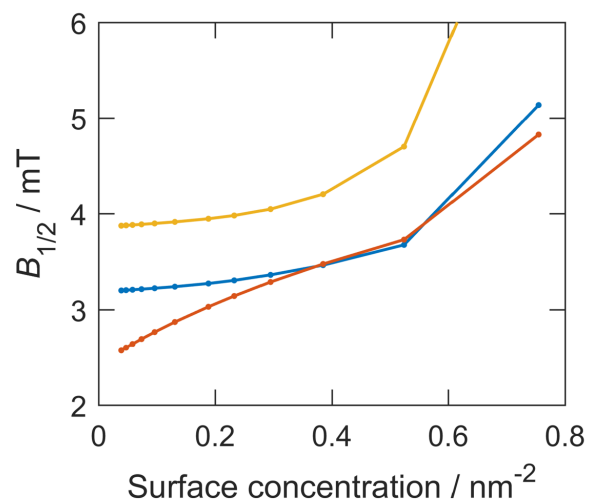


Figure S10: Characteristics of the low-field effect for orientationally averaged samples of circular microreactors containing three radicals at variable concentrations. Top: the magnetic field at which the low field effect occurs as a function of the surface concentration of the lipid radicals. Bottom: Magnetic field effect at the peak of the low-field feature. Parameters: $k_{P,0} = 0.2 \text{ ns}^{-1}$ and $k_e = 0.01 \text{ ns}^{-1}$, $J = 0$.

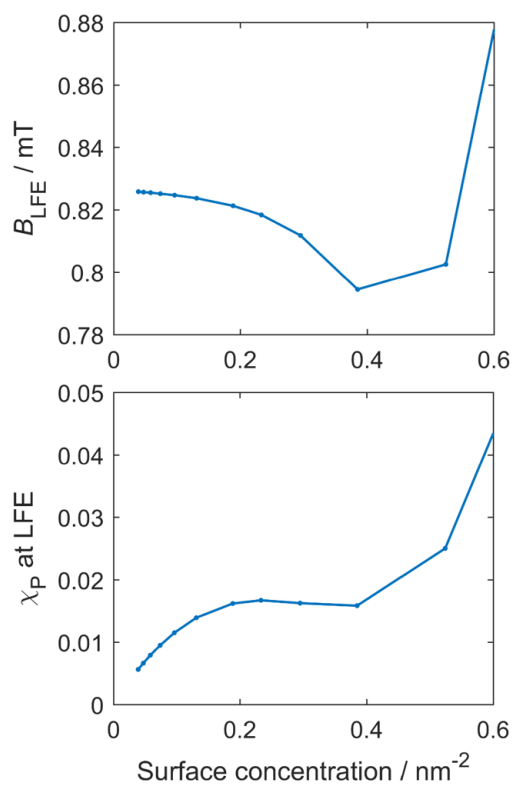
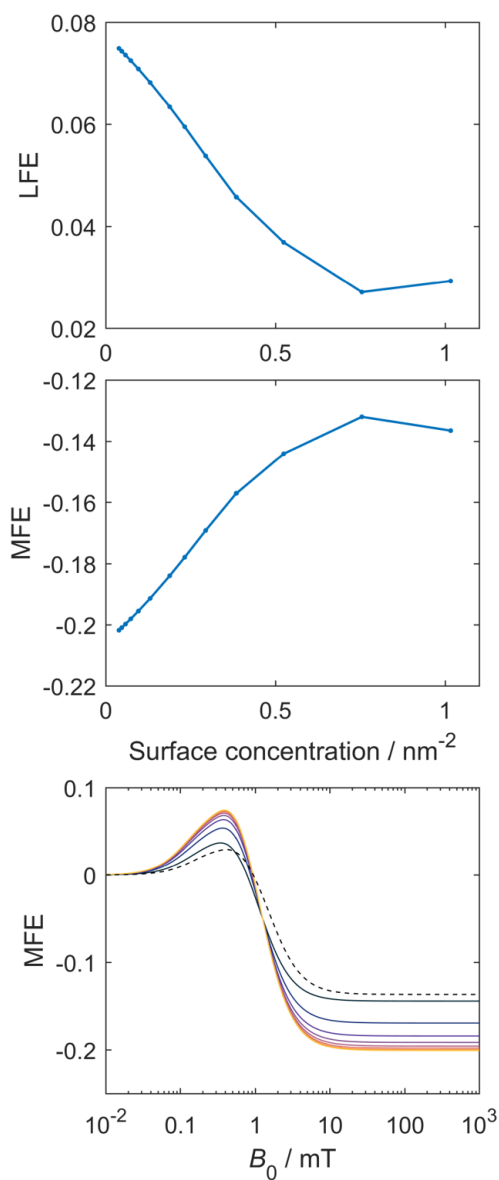


Figure S11: Characteristics of the magnetic field effect for circular microreactors containing three radicals at variable concentrations under the hypothetical scenario that the electron-electron dipolar interaction is absent. Top: the low field effect as a function of the surface concentration. Middle: the saturated magnetic field effect as a function of surface concentration. Bottom: the magnetic field effect as a function of the magnetic field. Parameters: $k_{P,0} = 0.2 \text{ ns}^{-1}$, $k_e = 0.01 \text{ ns}^{-1}$, $J = 0$ and $a = 10.3 \text{ MHz}$.



References

- [1] R. L. Donkers and D. G. Leaist. Diffusion of free radicals in solution. TEMPO, diphenylpicrylhydrazyl, and nitrosodisulfonate. *J. Phys. Chem. B*, 101(3):304–308, 1997.
- [2] M. Terazima, K. Okamoto, and N. Hirota. Transient radical diffusion in photoinduced hydrogen abstraction reactions of benzophenone probed by the transient grating method. *J. Phys. Chem.*, 97(50):13387–13393, 1993.
- [3] R. Macháň and M. Hof. Lipid diffusion in planar membranes investigated by fluorescence correlation spectroscopy. *Biochim. Biophys. Acta, Biomembr.*, 1798(7):1377–1391, 2010.
- [4] M. M. Gaschler and B. R. Stockwell. Lipid peroxidation in cell death. *Biochem. Biophys. Res. Commun.*, 482(2):419–425, 2017.
- [5] P. W. Atkins and D. Kivelson. ESR linewidths in solution. II. analysis of spin-rotational relaxation data. *J. Chem. Phys.*, 44:169–174, 01 1966.
- [6] M. Forbes, N. Lebedeva, R. C. White, T. K. Chen, R. Macarthur, P. Caregnato, and T. E. Hill. On the electron spin polarization observed in TREPR experiments involving hydroxyl and sulfate radicals. *Mol. Phys.*, 105:2127–2136, 08 2007.
- [7] M. C. R. Symons. Electron spin resonance spectra of organic oxy radicals. The radical $(\text{CH}_3)_3\text{CO}_3$. *J. Am. Chem. Soc.*, 91:5924, 1969.
- [8] J. B. Klauda, M. F. Roberts, A. G. Redfield, B. R. Brooks, and R. W. Pastor. Rotation of lipids in membranes: Molecular dynamics simulation, ^{31}P spin-lattice relaxation, and rigid-body dynamics. *Biophys. J.*, 94(8):3074 – 3083, 2008.
- [9] A. Kipriyanov Jr., A. Doktorov, and P. Purto. Magnetic field effects on bistability and bifurcation phenomena in lipid peroxidation. *Bioelectromagnetics*, 36(7):485–493, 2015.
- [10] N. C. Verma and R. W. Fessenden. Time resolved ESR spectroscopy. IV. detailed measurement and analysis of the ESR time profile. *J. Chem. Phys.*, 65:2139, 1976.
- [11] D. Becker, T. La Vere, and M. Sevilla. ESR detection at 77 K of the hydroxyl radical in the hydration layer of gamma-irradiated DNA. *Radiat. Res.*, 140:123–9, 11 1994.